PHYSICAL REVIEW D

PARTICLES AND FIELDS

THIRD SERIES, VOL. 1, NO. 9 1 MAY 1970

Reaction $K^+p \to K^+\pi^+\pi^-p$ at 2.53, 2.76, and 3.20 GeV/c†

G. S. ABRAMS,* L. EISENSTEIN, J. KIM, D. MARSHALL, T. A. O'HALLORAN, JR., W. SHUFELDT,‡ AND J. WHITMORE

University of Illinois, Urbana, Illinois 61801

(Received 12 January 1970)

The reaction $K^+p \to K^+p\pi^+\pi^-$ is studied at incident beam momenta of 2.53, 2.76, and 3.20 GeV/c, using the Argonne 30-in. hydrogen bubble chamber. Cross sections for the production of $K^{*0}(890)$, $N^{*++}(1236)$, and the double-resonance channel $K^+p \to K^{*0}(890)N^{*++}(1236)$ have been determined. We compare the production and decay angular distributions for the double-resonance channel with the predictions of several models which assume pion exchange. The decay angular distributions have also been compared with quark-model predictions. We find that none of the models tested completely accounts for all the features of the data. In addition, a low-mass enhancement in the $K\pi\pi$ system at 1300±10 MeV is observed.

I. INTRODUCTION

WE report the results of a study of the reaction $K^+p \to K^+\pi^+\pi^-p$ at 2.5, 2.7, and 3.2 GeV/c. The momenta were selected to study the K^+p interaction in the energy region of the $I=1$ enhancement reported at a center-of-mass energy of 2.505 GeV by Abrams *et al.*[1] and cover the energy region 2.44 to 2.68 GeV. No evidence has been observed in the four-particle final state for any resonant behavior in the K^+p system.

This reaction has been studied over a wide range of incident K^+ momenta from 1.2 to 12.7 GeV/c.[2–15] It is characterized by strong production of $K^{*0}(890)$ and $N^{*++}(1236)$. In addition, at momenta of 1.96 GeV/c and above, the simultaneous production of these resonances is observed. In the energy region reported in

† Work supported by the U.S. Atomic Energy Commission.

* Present address: Lawrence Radiation Laboratory, University of California, Berkeley, Calif.

‡ Present address: Physics Department, University of Wisconsin at Green Bay, Green Bay, Wisc.

[1] R. J. Abrams, R. L. Cool, G. Giacomelli, T. F. Kycia, B. A. Leontić, K. K. Li, and D. N. Michael, Phys. Rev. Letters **19**, 259 (1967).

[2] R. W. Bland, UCRL Report No. UCRL-18131, 1968 (unpublished).

[3] A. Bettini, M. Cresti, S. Limentani, L. Perruzzo, R. Santangelo, D. Locke, D. J. Crennell, W. T. Davies, and P. B. Jones, Phys. Letters **16**, 83 (1965). The published cross section has been scaled by a factor of 0.986 to agree with the total cross section due to Cool *et al.* (Ref. 29). (See R. W. Bland, Ref. 2.)

[4] M. G. Bowler, R. W. Bland, J. L. Brown, G. Goldhaber, J. A. Kadyk, V. Seeger, and G. H. Trilling, UCRL Report No. UCRL-16370, 1965 (unpublished).

[5] W. Chinowsky, G. Goldhaber, S. Goldhaber, T. O'Halloran, and B. Schwarzschild, Phys. Rev. **139**, B1411 (1965). The published cross sections have been scaled by a factor of 0.905 to agree with the total cross section due to Cool *et al.* (Ref. 29). (See R. W. Bland, Ref. 2.)

[6] G. Goldhaber, W. Chinowsky, S. Goldhaber, W. Lee, and T. O'Halloran, Phys. Letters **6**, 62 (1963).

[7] F. Bomse, S. Borenstein, J. Cole, D. Gillespie, R. Kraemer, G. Luste, I. Miller, E. Moses, A. Pevsner, R. Singh, and R. Zdanis, Phys. Rev. **158**, 1281 (1967).

[8] R. Newman, W. Chinowsky, J. Schultz, W. B. Johnson, and R. R. Larsen, Phys. Rev. **158**, 1310 (1967).

[9] M. Ferro-Luzzi, R. George, Y. Goldschmidt-Clermont, V. P. Henri, B. Jongejans, D. W. G. Leith, G. R. Lynch, F. Muller, and J. M. Perreau, Nuovo Cimento **39**, 417 (1965).

[10] R. George, Y. Goldschmidt-Clermont, V. P. Henri, B. Jongejans, M. Krammer, F. Muller, J. M. Pereau, W. DeBaere, J. Debaisieux, P. Dufour, F. Grard, J. Heughebaert, L. Pape, P. Peeters, F. Verbeure, and R. Windmolders, Nuovo Cimento **49A**, 9 (1967).

[11] W. DeBaere, J. Debaiseux, P. Dufour, F. Grard, J. Heughebaert, L. Pape, P. Peeters, F. Verbeure, R. Windmolders, G. Bassompierre, Y. Goldschmidt-Clermont, A. Grant, V. P. Henri, B. Jongejans, D. Linglin, W. Matt, F. Muller, J. M. Perreau, H. Piotrowska, I. Saitov, R. Sekulin, and G. Wolf, Nuovo Cimento **61A**, 397 (1969). The cross sections in this paper have been scaled by 1.08 to agree with the values given by G. Bassompierre *et al.*, Nucl. Phys. **B13**, 189 (1969).

[12] D. T. Gillespie, Ph.D. dissertation, Johns Hopkins University, Baltimore, Md., 1968 (unpublished).

[13] T. G. Trippe, University of California at Los Angeles Report No. UCLA-1026, 1968 (unpublished).

[14] J. Berlinghieri, M. S. Farber, T. Ferbel, B. Forman, A. C. Melissinos, T. Yamanouchi, and H. Yuta, Phys. Rev. Letters **18**, 1087 (1967).

[15] J. Berlinghieri, M. S. Farber, T. Ferbel, B. Forman, A. C. Melissinos, P. F. Slattery, and H. Yuta, Nucl. Phys. **B8**, 333 (1968).

TABLE I. Parameters of the exposure.

Nominal momentum (GeV/c)	Measured momentum (MeV/c)	Number of frames (in thousands)
2.53	2525±3	63
	2524±3	49
2.76	2753±3	109
	2775±3	52
3.20	3214±4	33
	3208±3	98
	3197±3	40

this paper, the quasi-two-body process $K^+p\to K^{*0}(890)N^{*++}(1236)$ is dominant, accounting for about 50% of the reaction. Our results are consistent with previous studies of this reaction above and below our energy range and indicate that this reaction is dominated by one-pion exchange. We have studied this quasi-two-body process in detail by examining the production angular distribution, the K^* and N^* decay angular distributions, and the correlations between the K^* and N^* decays. The results of these studies are compared with the predictions of various two-body production models based on single-meson exchange. We find that no one model completely accounts for all the features of the data. The angular correlations are also compared with quark-model predictions, and reasonable agreement is found for those predictions requiring only parity conservation in quark-quark scatterings.

Previous experiments at higher energies have reported a prominent enhancement in the $K^*\pi$ mass between 1.1 and 1.4 GeV.[16–23] Our energy region studies the threshold behavior of this enhancement. We find an enhancement in the low-mass $K\pi\pi$ system at 1300±10 MeV with a width of 80±20 MeV. The analysis is complicated by the $K^*(890)N^*(1236)$ background and it is difficult to make quantitative estimates of the cross section.

II. EXPERIMENTAL PROCEDURE

A. K^+ Beam

The Argonne National Laboratory 30-in. MURA hydrogen bubble chamber was exposed to the ZGS high-energy electrostatically separated beam[24] at nominal momenta of 2.5, 2.7, and 3.2 GeV/c. Accurate values of the beam momenta were obtained by fitting a subsample of the four-prong events to the four-constraint hypothesis:

$$K^+p\to K^+p\pi^+\pi^-. \quad (1)$$

The intrinsic width of the beam found in this study was consistent with the nominal momentum bite of ±1%. Table I shows the average fitted momentum at each beam setting.

Also shown in Table I is the number of frames of 70-mm film exposed at each momentum (four views per frame). The beam flux was measured by counting the number of three-prong beam associated events in a centrally chosen fiducial volume (see Sec. II D).

The light particle contamination in the beam was monitored continuously during the exposure by a threshold Čerenkov counter; this counter indicated that no more than 3% of the beam had velocities greater than that of a K^+ meson. A detailed study of π^+ contamination of the beam was performed at 3.2 GeV/c; at this momentum, 2000 frames were exposed to the beam tuned for transmission of π^+ mesons. By comparing the four-constraint fits in the four-prong topology in the π^+ film and in the K^+ film, we conclude that the π^+ contamination is less than 1% for each momentum. Using the selection criteria of Sec. II C, the contamination of the final state $K^+p\pi^+\pi^-$ by π^+-induced events is estimated to be less than 10 events at each momentum.

B. Event Processing

The film was scanned for all beam interactions or decays with two or more outgoing particles. A summary of the scanning results for the three- and four-prong topologies is given in Table II. All of the four-prong events were measured in three views on Scanning and Measuring Projectors (SMP's).

Spatial reconstruction and kinematic fitting of the measured events were performed using standard University of Illinois programs. Table III shows the results of a first-measurement pass of the film. These four-prong events satisfy the same fiducial volume and beam track criteria as the three-prong events used for the beam flux calculation.

[16] A recent review on the Q enhancement is given by G. Goldhaber, *Meson Spectroscopy* (Benjamin, New York, 1968), p. 209.
[17] G. Bassompierre, Y. Goldschmidt-Clermont, A. Grant, V. P. Henri, I. Hughes, B. Jongejans, R. L. Lander, D. Linglin, F. Muller, J. M. Perreau, I. Saitov, R. L. Sekulin, G. Wolf, W. DeBaere, J. Debaisieux, P. Dufour, F. Grard, J. Heughebaert, L. Pape, P. Peeters, F. Verbeure, R. Windmolders, M. Jobes, and W. Matt, Phys. Letters **26B**, 30 (1967).
[18] W. DeBaere, J. Debaiseux, P. Dufour, F. Grard, J. Heughebaert, L. Pape, P. Peeters, F. Verbeure, R. Windmolders, G. Fast, T. A. Filippas, Y. Goldschmidt-Clermont, V. P. Henri, B. Jongejans, W. Kock, F. Muller, and J. M. Perreau, Nuovo Cimento **49A**, 373 (1967).
[19] F. Bomse, S. Borenstein, A. Callahan, J. Cole, B. Cox, D. Ellis, L. Ettlinger, D. Gillespie, G. Luste, R. Mercer, E. Moses, A. Pevsner, and R. Zdanis, Phys. Rev. Letters **20**, 1519 (1968).
[20] B. C. Shen, I. Butterworth, C. Fu, G. Goldhaber, S. Goldhaber, and G. Trilling, Phys. Rev. Letters **17**, 726 (1966).
[21] G. Goldhaber, A. Firestone, and B. C. Shen, Phys. Rev. Letters **19**, 972 (1967).
[22] C. Y. Chien, P. M. Dauber, E. I. Malamud, D. J. Mellema, P. E. Schlein, P. A. Schreiner, W. E. Slater, D. H. Stork, H. K. Ticho, and T. G. Trippe, Phys. Letters **28B**, 143 (1968).
[23] M. S. Farber, T. Ferbel, P. F. Slattery, H. Yuta, University of Rochester Report No. UR-875-281, 1969 (unpublished).
[24] T. H. Fields, E. L. Goldwasser, and U. E. Kruse, Argonne National Laboratory Report No. THF/ELG/UEK-1, 1961 (unpublished).

TABLE II. Summary of scans for three- and four-prong events.

Momentum (GeV/c)	Fraction of film double scanned	Number of 3-prongs	Scanning efficiency for 3-prongs	Number of 4-prongs	Scanning efficiency for 4-prongs
2.53	0.56	1463	0.97±0.02	4411	0.99±0.01
2.76	0.22	2049	0.96±0.02	7574	0.98±0.02
3.20	0.86	1932	0.98±0.01	9480	0.99±0.01

While the reject rate indicated by Tables II and III (~12%) is consistent with rates from similar experiments performed at this laboratory, 300 rejected events at 3.2 GeV/c were remeasured to investigate possible systematic losses. Within statistics, all distributions from these remeasured events were consistent with those of first pass measurements.[25] Since the reject rate is low, we expect no significant biases to be introduced by omitting a complete remeasurement pass; cross sections have been corrected for this random loss of events.

C. Event Selection

All kinematic fits to the hypothesis $K^+p \to K^+p\pi^+\pi^-$ with a χ^2 probability greater than 0.001 were accepted. An event was considered ambiguous only if it had more than one fit satisfying this criterion, and if these fits had χ^2 probabilities within a factor of 25 of the best fit.

A sample of 600 events was used to test possible misidentification by comparing visually the ionization on the film with the ionization expected from the acceptable hypotheses. In no case could ionization criteria rule out an acceptable fit in favor of a hypothesis with one or more unseen neutral particles. Remeasurement of a random sample of four-prong events (~250 events) showed that the class of acceptable fits was stable under remeasurement.

At each momentum there were ~500 ambiguous events. At 3.2 GeV/c visual estimates of ionization showed that for ~65% of the resolvable ambiguous events choosing the hypothesis with the lowest χ^2 resulted in the correct choice. (75% of the ambiguous events were resolvable.) For the lower momenta, a minimum χ^2 decision was used to resolve the ambiguities; the effect of event misidentification is negligible since the ambiguity classes are a small fraction of the total number of events.

TABLE III. Summary of film measurement.

Momentum (GeV/c)	Number of rejects	Number of $K^+p\pi^+\pi^-$
2.53	560	2971
2.76	800	4872
3.20	1260	5150

[25] Substantial remeasurements were performed for the two-prong and two-prong-plus-V-topologies. Analysis of the remeasured events did not offer significant evidence for further measurements in the four-prong topology.

D. Cross Sections

The cross section was determined at each energy by normalizing the number of events in a central fiducial volume corrected for scanning and measurement loss to the number of three-prong decay events satisfying the same beam criteria. The branching ratio used was 0.060±0.001.[26] The cross sections are given in Table IV.

III. GENERAL FEATURES OF THE REACTION

The dominant features of reaction (1) are shown in Figs. 1–3, where we plot the mass of the $K^+\pi^-$ pair versus the $p\pi^+$ pair. It is clear that the dominant process is the copious production of $K^*(890)$ and $N^*(1236)$.

In order to determine the cross sections for the dominant final states of this reaction a maximum-likelihood analysis of the triangle plot was performed using the computer program MINFUN.[27] We have used four non-

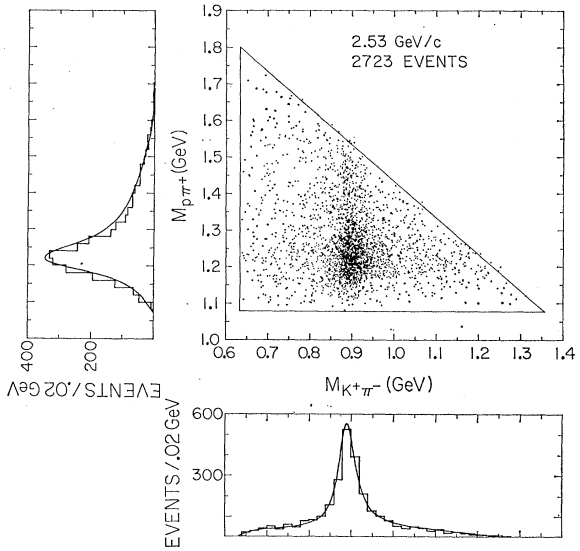

FIG. 1. Scatter diagram of the invariant masses of the $K^+\pi^-$ and $p\pi^+$ systems for 2.53 GeV/c. The solid curves on the mass projections are the result of the maximum-likelihood fits whose parameters are summarized in Table IV.

[26] G. Trilling, UCRL Report No. UCRL-16473, 1965 (unpublished).

[27] W. Humphrey and B. Cottrell, UCRL Physics Notes, Memo No. P-6, rev., 1966 (unpublished).

TABLE IV. Maximum-likelihood solutions for the dominant channels in $K^+p\pi^+\pi^-$ production.

Channel	2.53 GeV/c Fraction (%)	2.53 GeV/c Cross section (mb)	2.76 GeV/c Fraction (%)	2.76 GeV/c Cross section (mb)	3.20 GeV/c Fraction (%)	3.20 GeV/c Cross section (mb)
$K^*(890)p\pi^+$	11.3±1.6	0.25±0.04	12.8±1.3	0.29±0.04	15.7±1.3	0.34±0.05
$K^+\pi^-N^*(1236)$	18.1±1.7	0.39±0.06	15.5±1.3	0.35±0.05	21.2±1.3	0.45±0.05
$K^*(890)N^*(1236)$	51.7±1.3	1.13±0.11	51.6±1.4	1.17±0.10	44.2±1.4	0.96±0.08
$K^+p\pi^+\pi^-$ (nonresonant)	18.9±1.7	0.41±0.06	20.1±1.3	0.46±0.05	18.9±1.3	0.41±0.06
Total		2.18±0.17		2.27±0.18		2.17±0.17

interfering amplitudes corresponding to the processes

$$K^+p\rightarrow K^{*0}(890)p\pi^+ \quad (1a)$$

$$\rightarrow K^+\pi^-N^{*++}(1236) \quad (1b)$$

$$\rightarrow K^{*0}(890)N^{*++}(1236) \quad (1c)$$

$$\rightarrow K^+p\pi^+\pi^-(\text{nonresonant}). \quad (1d)$$

The results of the fitting are given in Table IV and shown in Figs. 1–3. The events not belonging to K^*N^* reactions are assumed to be distributed according to their phase space. Relativistic p-wave Breit-Wigner amplitudes were used for the K^* and N^*.[28] We have also used the accepted values of the mass and width for the $K^*(890)$ and $N^*(1236)$. The $p\pi^+$ mass projections in Figs. 1–3 indicate that the observed $N^*(1236)$ mass is approximately 10 MeV lower than the accepted value. However, the percentage fits in Table IV are not sensitive to this difference.

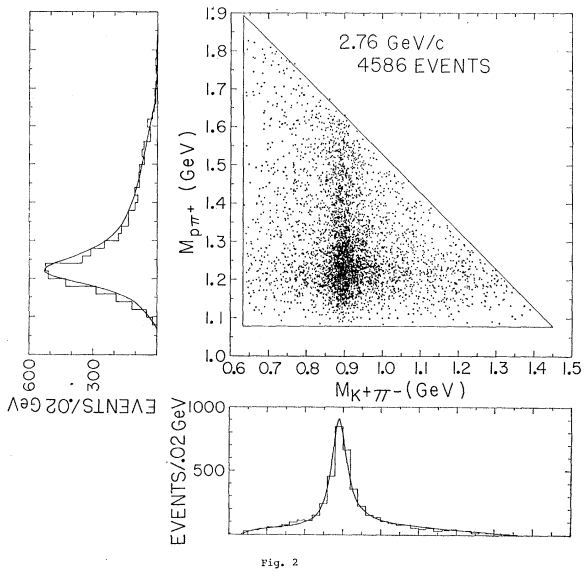

FIG. 2. Scatter diagram of the invariant masses of the $K^+\pi^-$ and $p\pi^+$ systems for 2.76 GeV/c. The solid curves on the mass projections are the result of the maximum-likelihood fits whose parameters are summarized in Table IV.

[28] J. D. Jackson, Nuovo Cimento **34**, 1644 (1964).

At 3.2 GeV/c we tried fitting the triangle plot to six noninterfering amplitudes. The additional two amplitudes tried were

$$K^+p\rightarrow K^{*0}(1420)p\pi^+ \quad (1e)$$

$$\rightarrow K^{*0}(1420)N^{*++}(1236). \quad (1f)$$

This fit yielded (1.2±0.7)% for (1e) and (1.3±0.7)% for the percentage of (1f). As expected, the fraction of $N^*K^+\pi^-$ and phase space decreased by similar amounts to accommodate this $K^*(1420)$ production. (These are the processes that populate the high-mass region of the $K\pi$ mass spectrum.) From this we measure a cross section of 55±30 μb for $K^{*0}(1420)$ production and decay into $K^+\pi^-$ at 3.2 GeV/c in this final state.

Our cross sections for reaction (1) and for the quasi-two-body final state are shown in Fig. 4 with the results from other experiments. The cross section for the reaction $K^+p\rightarrow K^+\pi^+\pi^-p$ is observed to increase with p_{lab} until it is above the K^*N^* threshold and then have a slight decrease as a function of laboratory momentum. It is interesting to note, however, that the major part

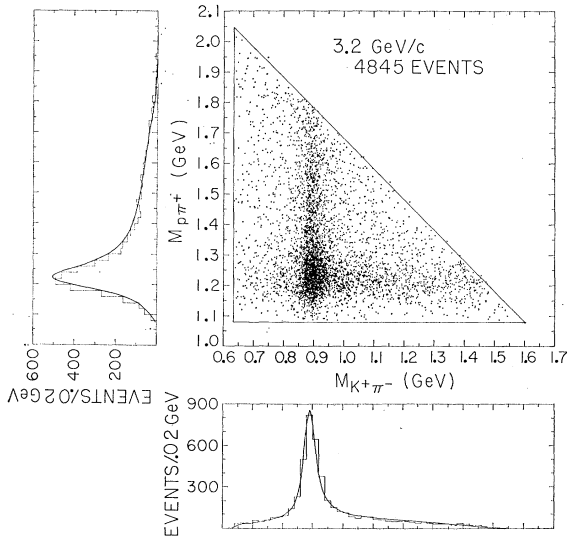

FIG. 3. Scatter diagram of the invariant masses of the $K^+\pi^-$ and $p\pi^+$ systems for 3.20 GeV/c. The solid curves on the mass projections are the result of the maximum-likelihood fits whose parameters are summarized in Table IV.

of the $\sigma(K^+\pi^+\pi^-p)$ energy dependence is due to the energy dependence of the K^*N^* final state. The dashed curve in Fig. 4 is a fit of the K^*N^* cross section between 2.65 and 5.44 GeV/c to the form $\sigma=\sigma_0 p_{\rm lab}{}^{-N}$. This fit yields $\sigma_0=3.6\pm0.7$ mb, $N=1.1\pm0.1$ As shown in Fig. 4, the remaining part of the cross section is essentially flat between 2.5 and 13.0 GeV/c. The initial increase of the cross section for the $K^+p\pi^+\pi^-$ final state is coincident with the enhancement reported by Cool *et al.*[29] at 1.9 ± 0.02 GeV.

IV. REACTION $K^+p\to K^{*0}N^{*++}$

A. K^*N^* Differential Cross Sections

The large accumulation of events in the $K^{*0}(890)-N^{*++}(1236)$ overlap region of the triangle plots at all three momenta enables us to perform a detailed study of the production mechanism for the reaction

$$K^+p\to K^{*0}N^{*++}$$
$$\searrow$$
$$K^+\pi^-.$$

In Fig. 5 we present the differential cross sections for each momentum. To avoid a kinematic dip at small values of Δ^2 (arising from the finite widths of the K^* and N^*) we have plotted the data as a function of $\cos\theta_{\rm c.m.}$, the cosine of the angle between the K^* and the incoming K^+ meson in the K^+p center-of-mass system. For convenience we have included in Fig. 5 scales for Δ^2, where the value of Δ^2 for a given value of $\cos\theta_{\rm c.m.}$ is taken at the central values of the resonance positions.

The differential cross sections have been calculated by fitting the triangle plot densities (see Sec. III) over intervals in the $\cos\theta_{\rm c.m.}$ variable between 0.8 and 1.0. This gives the K^*N^* population of each $\cos\theta_{\rm c.m.}$ bin. (For example at 3.2 GeV/c we have measured a K^*N^* purity of 97% near $\cos\theta_{\rm c.m.}=1.0$ and a purity of 77% near $\cos\theta_{\rm c.m.}=0.8$.) It should be noted that this method may be more reliable than that of using mass selection criteria [e.g., $840<M(K^+\pi^-)<940$ MeV and $1120<M(p\pi^+)<1320$ MeV] to obtain the shape of the differential cross section. Although the background (non-K^*N^* events) with these cuts is small (less than 5% at 3.2 GeV/c for $\cos\theta_{\rm c.m.}>0.8$), there is considerable variation in the percentage of background as a function of $\cos\theta_{\rm c.m.}$ for $\cos\theta_{\rm c.m.}>0.8$. The effect of neglecting this background variation would be to flatten out the production angular distribution.

The data are seen to be consistent with an exponential falloff as a function of production cosine. From a least-squares fit to the data (for $\cos\theta_{\rm c.m.}>0.8$) we have measured the slopes A [assuming a functional form $d\sigma/d\Omega\sim\exp(A\cos\theta_{\rm c.m.})$] to be 7.7 ± 0.7, 11.6 ± 0.8, and 15.2 ± 1.0 at 2.53, 2.76, and 3.20 GeV/c, respectively.

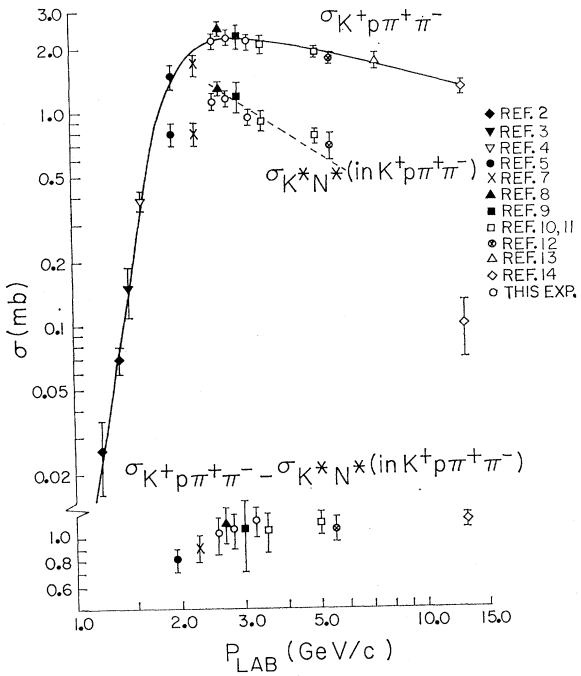

FIG. 4. Cross sections of the reactions $K^+p\to K^+p\pi^+\pi^-$ and $K^+p\to K^{*0}N^{*++}$ ($K^{*0}\to K^+\pi^-$), and their difference, as a function of laboratory momentum. The solid curve is hand drawn through the data points. The dashed curve is the result of the fit to the K^*N^* cross section described in the text.

Using the central mass values for the K^* and N^*, these correspond to values of 6.7 ± 0.6, 7.7 ± 0.5, and 7.9 ± 0.5 $(\text{GeV}/c)^{-2}$, respectively, for the slopes in $d\sigma/d\Delta^2$.

At other energies K^*N^* production has been found to be dominated by pion exchange in the t channel. We have compared the data with three refined models[5] of pion exchange; the form-factor model of Dürr and Pilkhun, the absorptive model of Gottfried and Jackson, and the Reggeized model of Frautschi and Jones. We find that none is completely successful in describing the differential cross sections at small Δ^2.

The cross section for one-pion exchange in the reaction $K^+p\to K^{*0}N^{*++}$, $K^{*0}\to K^+\pi^-$ is given by[30]

$$\frac{d\sigma}{d\Omega}=(\hbar c)^2\times\frac{2}{3}\frac{1}{s}\frac{P_{K^*}}{P_{K^+}}\frac{g^2}{4\pi}\frac{G^2}{4\pi}\frac{1}{(m_\pi{}^2+\Delta^2)^2}\frac{1}{4m_{K^*}{}^2}$$
$$\times[\Delta^2+(m_{K^*}-m_K)^2](4m_{N^*}{}^2m_\pi{}^2)^{-1}$$
$$\times[\Delta^2+(m_{N^*}-m_p)^2][\Delta^2+(m_{N^*}+m_p)^2]^2, \quad (2)$$

where

$$g^2/4\pi=2\Gamma_{K^*}M_{K^*}{}^2/3q_{K;K^*}{}^3=1.0$$

for

$$\Gamma_{K^*}=0.049\text{ GeV},\quad M_{K^*}=0.892\text{ GeV}$$

and

$$\frac{G^2}{4\pi}=\frac{\Gamma_{N^*}6m_\pi{}^2m_{N^*}{}^2}{(m_{N^*}+m_p)^2-m_\pi{}^2}(q_{p;N^*}{}^3)^{-1}=0.043$$

[29] R. L. Cool, G. Giacomelli, T. F. Kycia, B. A. Leontić, K. K. Li, A. Lundby, and J. Teiger, Phys. Rev. Letters **17**, 102 (1966).

[30] J. D. Jackson and H. Pilkuhn, Nuovo Cimento **33**, 906 (1964).

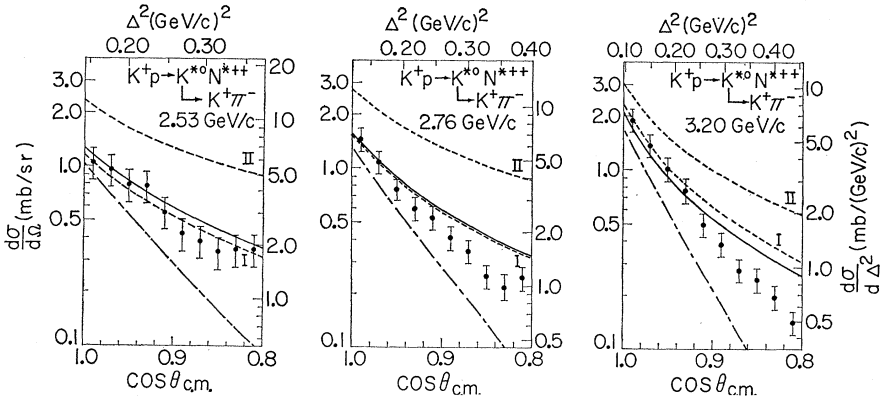

FIG. 5. Differential cross section for the reaction $K^+p\to K^{*0}N^{*++}$ ($K^{*0}\to K^+\pi^-$) for the three momenta 2.53, 2.76, and 3.20 GeV/c. The solid curve is the result of an OPE calculation with Dürr-Pilkuhn vertex factors and a form factor. The dashed curves are the results of OPEA calculations with parameters given in Table V. The dot-dashed curves are the result of a Reggeized pion calculation of Frautschi and Jones in which $b=0.001$ is used.

for

$$\Gamma_{N^*}=0.140\text{ GeV},\quad M_{N^*}=1.236\text{ GeV}.$$

s is the square of the center-of-mass energy, P_{K^+} and P_{K^*} are the center-of-mass momenta of the incident K^+ and outgoing K^*, respectively, and $q_{A;B}$ represents the momentum of particle A in the rest frame of particle B. It is well known that this calculation disagrees with the observed data in magnitude and shape.

Dürr and Pilkuhn[31] have modified (2) by the inclusion of off-mass-shell vertex factors and a form factor. The result of this modification is that the differential cross section given by (2) is multiplied by

$$\frac{1+R_{N^*}{}^2q_{N^*}{}^2(\text{on})}{1+R_{N^*}{}^2q_{N^*}{}^2(\text{off})}\,\frac{1+R_{K^*}{}^2q_{K^*}{}^2(\text{on})}{1+R_{K^*}{}^2q_{K^*}{}^2(\text{off})}\left(\frac{\alpha^2-m_\pi{}^2}{\alpha^2+\Delta^2}\right)^2,$$

where $q_R$off is the momentum of the exchanged pion in the resonance (R) rest frame and $q_R$on is the momentum it would have if its mass were that of a physical pion. We have used the following parameters:

$$R_{N^*}=4.0\,(\text{GeV}/c)^{-1},\qquad R_{K^*}=1.25\,(\text{GeV}/c)^{-1},$$

and

$$\alpha^2=2.3\,(\text{GeV}/c)^2,$$

as determined by Trippe[13] from a fit to K^*N^* production from 3 to 13 GeV/c.

The results of this calculation are shown by the solid curves in Fig. 5. The model is seen to describe the data well near $\Delta_{\min}{}^2$, but to fall off too slowly with increasing Δ^2 to fit the data. In addition, the decay angular distributions predicted by this model [which are the same as those predicted by simple one-pion exchange (OPE)] do not agree with those experimentally observed (see Sec. IV B).

The dashed curves in Fig. 5 are the results of a one-pion-exchange model with absorptive (OPEA) corrections[32–35] calculated using the exact summation of the partial-wave method of Donohue and Keyser.[36]

In this model the partial-wave Born amplitude for simple pion exchange is multiplied by the product of the square root of the elastic scattering S-matrix elements in the initial and final states. Assuming that elastic scattering is purely diffractive and helicity nonchanging, one modifies the partial-wave Born amplitude as follows:

$$M_{fi}{}^J=(S_{ff}{}^J)^{1/2}B_{fi}{}^J(S_{ii}{}^J)^{1/2},\tag{3}$$

where

$$S_{ii}{}^J=1-C_i\exp[-\gamma_i(J-\tfrac{1}{2})^2]$$

and

$$C_1=\sigma_T{}^i/4\pi A_i,\qquad \gamma_i=1/(2q_i{}^2A_i).$$

$\sigma_T{}^i$ is the K^+p total cross section, A_i is the slope of the

TABLE V. Absorption model parameters.

P_{lab} (GeV/c)	C_i (expt)	γ_i (expt)	I C_i	I γ_i	I C_f	I γ_f	II C_i	II γ_i	II C_f	II γ_f
2.53	1.05±0.04	0.156±0.005	1.0	0.16	1.0	0.03	0.9	0.16	0.9	0.08
2.76	1.15±0.06	0.154±0.008	1.0	0.15	1.0	0.03	0.9	0.15	0.9	0.075
3.20	0.95±0.05	0.108±0.006	1.0	0.10	1.0	0.03	0.9	0.10	0.9	0.05

[31] H. P. Dürr and H. Pilkuhn, Nuovo Cimento **40**, 899 (1965).
[32] K. Gottfried and J. D. Jackson, Nuovo Cimento **33**, 309 (1964).
[33] K. Gottfried and J. D. Jackson, Nuovo Cimento **34**, 735 (1964).
[34] J. D. Jackson, J. T. Donohue, K. Gottfried, R. Keyser, and B. E. Y. Svensson, Phys. Rev. **139**, B428 (1965).
[35] J. T. Donohue, Ph.D. thesis, University of Illinois, 1967 (unpublished).
[36] The calculations were done using a program described by R. Keyser, CERN Report No. DD/CO/66/3 (unpublished). The program was modified at the University of Illinois to perform the calculations to obtain the correlation coefficients for double-resonance production.

forward K^+p elastic scattering diffraction peak, q_i is the incident center-of-mass momentum, and J is the total angular momentum. Analogous definitions apply to the final-state parameters C_f and γ_f. From measurements of the elastic scattering[37] and the total cross sections[1] at our energies, we have determined the parameters C_i(expt) and γ_i(expt), which are given in Table V. It has been customary to take $C_f=1$ and $\gamma_f=(0.5-0.75)\gamma_i$, corresponding to total absorption of the lowest partial wave and a larger Gaussian region of absorption in the final state. For initial-state absorption parameters fixed (we use $C_i=1.0$ at all energies), best agreement with differential cross-section measurements is obtained for the parameter set labelled I in Table V. At all momenta, the shapes of the differential cross sections are similar to those predicted by the form-factor model, and are similarly inadequate. The same kind of results could be obtained for γ_f larger (and $\sim\gamma_i$) if we were to use values of γ_i smaller by about a factor of 2. According to the parametrization used in the absorption model, this would imply a slope in K^+p elastic scattering twice as large as that experimentally observed. However, as discussed in Sec. IV B, the parameter sets that best fit the differential cross section do *not* give the best agreement with the decay angular distributions. A better fit to the decay angular distributions is obtained by using the set of parameters designated II in Table V and is shown as the dashed curve labelled II in Fig. 5.

A Reggeized pion-exchange calculation[38] is shown by the dot-dashed curves in Fig. 5. The predictions of this model, which assume that only one helicity amplitude dominates, are seen to be too steep when compared with the data. As shown in Fig. 6, our data along with those of Goldschmidt-Clermont *et al.*[39] exhibit the

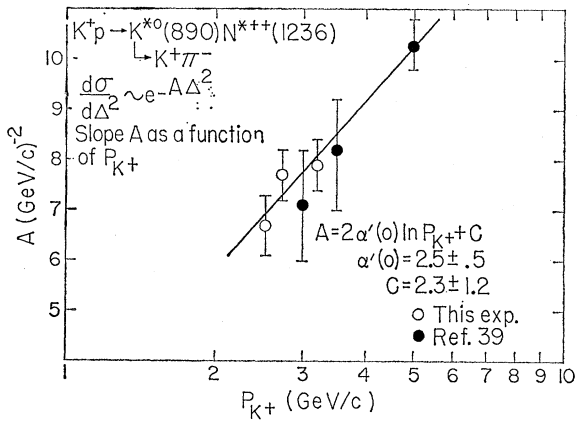

FIG. 6. Slope for process $K^+p\to K^{*0}N^{*++}$ ($K^{*0}\to K^+\pi^-$) as a function of laboratory momentum.

expected Regge shrinkage, but the large value of $\alpha'(0)_{\text{eff}}$ that the data indicate [2.5 ± 0.5 $(\text{GeV}/c)^{-2}$] does not appear consistent with the usual value of 1 $(\text{GeV}/c)^{-2}$. This value for the effective slope of the pion trajectory is obtained by neglecting any Δ^2 dependence of the residue function and signature factor (which certainly is important for pion exchange) and fitting the momentum dependence of the slope A of K^*N^* production to the form

$$A=2\alpha'(0)\ \ln P_{K^+}+C,$$

where C has been determined to be 2.3 ± 1.2 $(\text{GeV}/c)^{-2}$.

B. K^*N^* Decay Angular Distributions

The decay angular distributions of the $K^{*0}\to K^+\pi^-$ and $N^{*++}\to p\pi^+$ decays have been studied to yield information about the production mechanism of the reaction

$$K^+p\to K^{*0}N^{*++}.$$

As shown by Pilkuhn and Svensson[40] and by Donohue,[35,41] the joint decay distribution of the K^*N^* system is described by angular functions with 19 parameters. The 19 parameters are the six single-particle density-matrix elements and 13 coefficients (R_4 and R_9–R_{20}).

We use the notation of Donohue to describe the joint decay distribution

$$\begin{aligned}W(\theta_{K^*}\phi_{K^*};\theta_{N^*}\phi_{N^*})=(1/16\pi^2)\{&1+\tfrac{1}{2}(1-3\rho_{00}{}^{K^*})\\
&\times(1-3\cos^2\theta_{K^*})-\tfrac{1}{2}(1-4\rho_{33}{}^{N^*})(1-3\cos^2\theta_{N^*})\\
&+\tfrac{1}{2}R_4(1-3\cos^2\theta_{K^*})(1-3\cos^2\theta_{N^*})\\
&-3(\rho_{1,-3}{}^{K^*}\sin^2\theta_{K^*}\cos2\phi_{K^*}\\
&+\sqrt{2}\,\mathrm{Re}\rho_{10}{}^{K^*}\sin2\theta_{K^*}\cos\phi_{K^*})\\
&-2\sqrt{3}\,(\mathrm{Re}\rho^{N^*}{}_{3,-1}\sin^2\theta_{N^*}\cos2\phi_{N^*}\\
&+\mathrm{Re}\rho_{31}{}^{N^*}\sin2\theta_{N^*}\cos\phi_{N^*})\\
&-3(1-3\cos^2\theta_{N^*})[R_9\sin^2\theta_{K^*}\cos2\phi_{K^*}\\
&+(1/\sqrt{2})R_{10}\sin2\theta_{K^*}\cos\phi_{K^*}]\\
&-\sqrt{3}\,(1-3\cos^2\theta_{K^*})(R_{11}\sin^2\theta_{N^*}\cos2\phi_{N^*}\\
&+R_{12}\sin2\theta_{N^*}\cos\phi_{N^*})+3\sqrt{3}\,(\sin^2\theta_{K^*}\sin^2\theta_{N^*}\\
&\times[R_{13}\cos(2\phi_{K^*}+2\phi_{N^*})+R_{14}\cos(2\phi_{K^*}-2\phi_{N^*})])\\
&+\sin^2\theta_{K^*}\sin2\theta_{N^*}[R_{15}\cos(2\phi_{K^*}+\phi_{N^*})\\
&+R_{16}\cos(2\phi_{K^*}-\phi_{N^*})]+(1/\sqrt{2})\sin2\theta_{K^*}\sin^2\theta_{N^*}\\
&\times[R_{17}\cos(\phi_{K^*}+2\phi_{N^*})+R_{18}\cos(\phi_{K^*}-2\phi_{N^*})]\\
&+(1/\sqrt{2})\sin2\theta_{K^*}\sin2\theta_{N^*}\\
&\times[R_{19}\cos(\phi_{K^*}+\phi_{N^*})+R_{20}\cos(\phi_{K^*}-\phi_{N^*})]\},\end{aligned}\tag{4}$$

[37] J. Whitmore, University of Illinois (private communication).
[38] S. Frautschi and L. Jones, Phys. Rev. **164**, 1918 (1967).
[39] Y. Goldschmidt-Clermont, V. P. Henri, B. Jongejans, A. Moisseev, F. Muller, J. M. Perreau, A. Prokes, V. Yarba, W. DeBaere, J. Debaisieux, P. Dufour, F. Grard, J. Heughebaert, L. Pape P. Peeters, F. Verbeure, and R. Windmolders, Nuovo Cimento **46**, 539 (1966).
[40] H. Pilkuhn and B. E. Y. Svensson, Nuovo Cimento **38**, 518 (1965).
[41] J. T. Donohue, Nuovo Cimento **52A**, 1152 (1967).

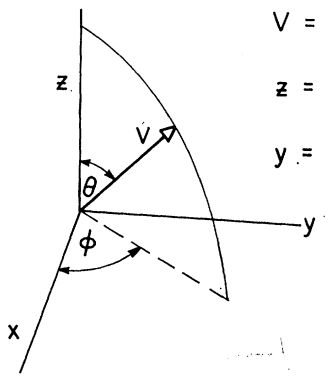

$V = \left[K^+_{out}, p_{out} \right]$ K*or N*rest frame

$z = \left[K^+_{in}, p_{in} \right]$ K*or N*rest frame

$y = \left[K^+_{in} \times K^*, p_{in} \times N^* \right]$ c.m.s.

$$W_{K^*}(\cos\theta,\phi) = \frac{3}{4\pi}\left[\rho_{0\,0}\cos^2\theta + \tfrac{1}{2}(1-\rho_{0\,0})\sin^2\theta - \rho_{1,-1}\sin^2\theta\cos 2\phi - \sqrt{2}\,\mathrm{Re}\rho_{1\,0}\sin 2\theta\cos\phi \right]$$

$$W_{N^*}(\cos\theta,\phi) = \frac{3}{4\pi}\left[\rho_{3\,3}\sin^2\theta + (\tfrac{1}{2}-\rho_{3\,3})(\tfrac{1}{3}+\cos^2\theta) - \frac{2}{\sqrt{3}}\mathrm{Re}\rho_{3\,1}\sin 2\theta\cos\phi \right.$$

$$\left. - \frac{2}{\sqrt{3}}\mathrm{Re}\rho_{3,-1}\sin^2\theta\cos 2\phi \right]$$

FIG. 7. Coordinate system defining the decay angles of the heavier decay product in the resonance rest frame. W_{K^*} and W_{N^*} are the expected K^* and K^* decay angular distributions expressed in terms of the spin density-matrix elements $\rho_{m,m'}$.

where R_4 and R_9–R_{20} are linear functions of the real part of the joint decay density matrix $\rho_{mm';bb'}$. The coordinate system is that shown in Fig. 7 and m and m' are the magnetic quantum numbers referring to the K^*, and $\frac{1}{2}n$ and $\frac{1}{2}n'$ are those referring to the N^*. The explicit functions are given in Table VI, where we have defined

$$R_{mm';nn'} = \mathrm{Re}\rho_{mm';nn'}.$$

In terms of the 19 parameters [in Eq. (4)] the predictions of the simple OPE model become

$$\rho_{00}=1, \qquad R_4=1$$

and all other coefficients zero.

Figure 8 shows the separate $\cos\theta_{K^*}$, ϕ_{K^*}, $\cos\theta_{N^*}$, and ϕ_{N^*} decay angular distributions at each of the three energies for $\cos\theta_{c.m.}>0.8$ For this study we define K^*N^* events by restricting the $K^+\pi^-$ mass to the interval 840–940 MeV and the $p\pi^+$ mass to the interval 1120–1320 MeV. The solid curves are the results of fitting these distributions to the appropriately integrated form of Eq. (4). The curves adequately represent the features of the data except for the large asymmetry present at all energies in the $\cos\theta_{K^*}$ distribution. In Fig. 9 we show this asymmetry (as measured by $\langle Y_1^0 \rangle$) as a function of the mass of the $K\pi$ system. This asymmetry is a rapidly varying function of $K\pi$ mass, reaching a maximum for $M_{K\pi}\sim 0.84$ GeV and going to zero for $M_{K\pi}\sim 0.93$ GeV. This figure also shows that the asymmetry is largest for $K\pi$ systems peripherally produced with the N^*. The above formalism, which assumes that the K^* and N^* are free-spin 1^- and $\frac{3}{2}^+$ particles that are produced and decay via parity conserving interactions, cannot account for this asymmetry. However, it is still of interest to see whether the various models, which are based on these assumptions, can correctly account for the other features of K^*N^* production.[42]

The data in Fig. 8 indicate that the single-particle density-matrix elements ρ_{00}, $\rho_{1,-1}$, ρ_{33}, and $\mathrm{Re}\rho_{3,-1}$, in the production cosine range of 0.8 to 1.0, are similar at all three energies. In Table VI we show that this is true for all 19 parameters.[43]

A comparison with the data at 5 GeV/c [11] shows that this feature of the data extends to higher momenta. In agreement with the CERN group, we observe significant differences from simple OPE predictions for ρ_{00}, ρ_{33}, $\mathrm{Re}\rho_{10}$, R_4, R_{13}, and R_{19} (though only at 3.2 for the last term).

In Figs. 10 and 11 we present the 19 parameters measured at a three momenta as a function of $\cos\theta_{c.m.}$[44] and compare them with the predictions of the one-pion-

[42] To assure ourselves that a comparison of theory and experiment is not affected by the presence of the K^* asymmetry, we have performed all the analyses described below separately on the events with $\cos\theta_{K^*}>0$ and $\cos\theta_{K^*}<0$. Within the limits of our statistics no differences in the parameters obtained for these two sets were observed. We have also applied more restrictive mass selections on the $K^+\pi^-$ and $p\pi^+$ systems. Again no differences in the parameters were observed.

[43] All matrix elements were obtained from the data by the method of moments, using the selection criteria previously defined.

[44] The amount of background present in each of the four production cosine intervals has been determined. At 3.2 GeV/c, the percentage of background is 3% for $0.98<\cos\theta_{c.m.}<1.0$, 3% for $0.94<\cos\theta_{c.m.}<.98$, 12% for $0.88<\cos\theta_{c.m.}<0.94$, and 17% for $0.80<\cos\theta_{c.m.}<0.88$. At the other energies the background levels are comparable. However, no background subtraction was performed.

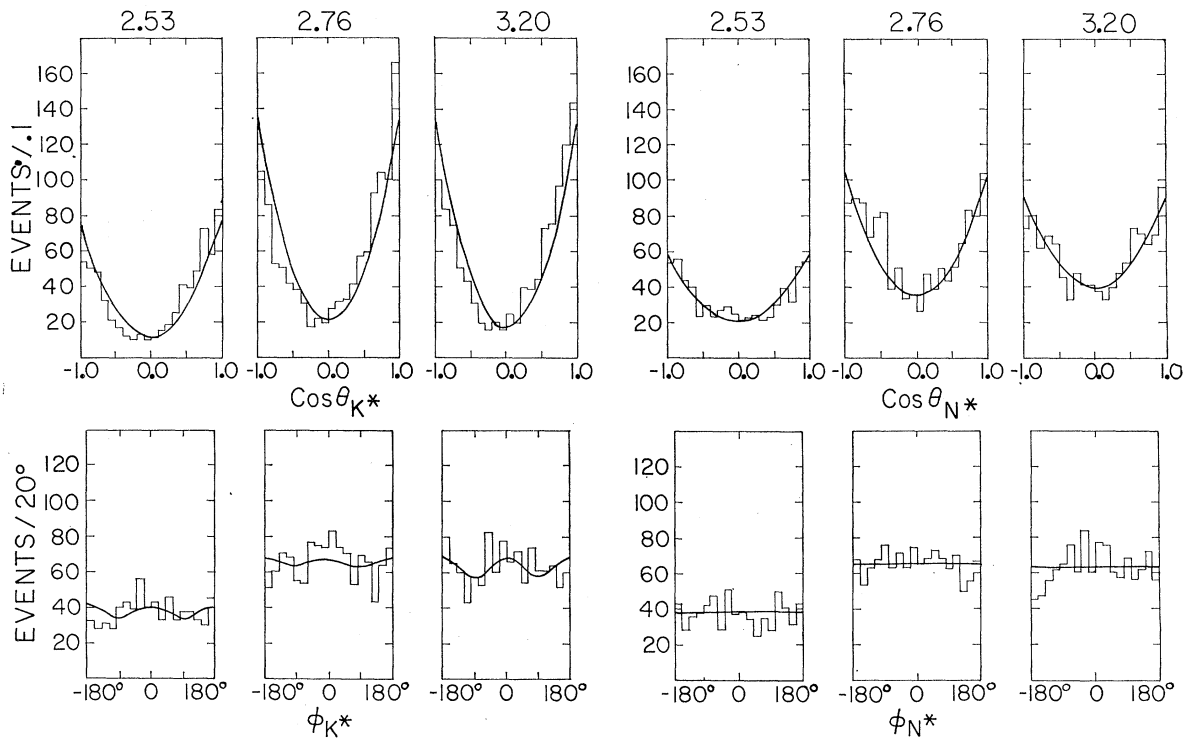

FIG. 8. Decay angular distributions of the selected (0.84 GeV$<M_{K^+\pi^-}<$0.94 Gev, 1.12 GeV$<M_{p\pi^+}<$1.32 GeV, cos$\theta_{c.m.}>$0.8) double-resonance events. The solid curves are the result of a moment analysis with parameters given in Table VI.

exchange model with absorption (OPEA). The solid curves are obtained by using the parameter sets given by II in Table V. (The predictions of these sets are determined mainly by $C_i \sim C_f \sim 0.9$ and not by the precise values for γ_i and γ_f.) For comparison we also display (dashed curves) the predictions given by parameter sets I (those sets that gave best agreement with differential cross section and agree with experimentally determined values for γ_i and C_i). We observe that the only significant differences between the two sets of parameters is for ρ_{00}.

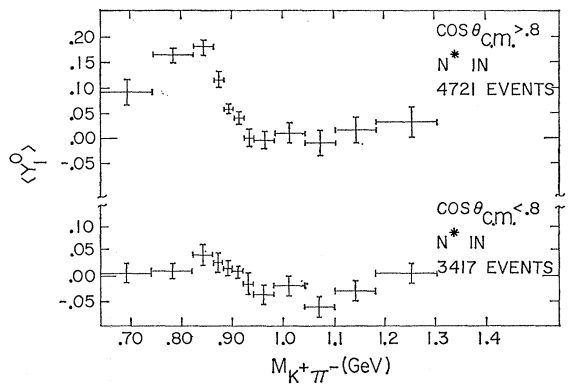

FIG. 9. $[Y_1^0]$ as a function of $K\pi$ mass for N^{*++} in (1.12$<M_{p\pi^+}<$1.32 GeV), cos$\theta_{c.m.}>$0.8, and cos$\theta_{c.m.}<$0.8.

We note that this model specifies correctly which of the interparticle correlation terms should be large (R_4, R_{12}, R_{13}, and R_{19}) and which should be small (R_9–R_{11}, R_{14}–R_{18}, and R_{20}), and agrees well with the data in both magnitude and sign for the large terms. The model is also somewhat successful for the single-particle spin density-matrix elements, failing to reproduce the behavior of only $\rho_{1,-1}$ and Reρ_{10}.

In order to determine whether better agreement between experimental data and the OPEA predictions could be obtained, we have studied the sensitivity of the absorptive peripheral model to variations in both the initial- and final-state absorption parameters. Varying C_i and C_f between 0.5 and 1 and γ_i and γ_f between 0.02 and 0.32 produced no set which gave complete agreement for all distributions. For example, *no choice* of parameters gave Reρ_{10} as large and as negative as the data or displayed the behavior in the magnitude R_{19} as a function of momentum transfer. In addition, as previously mentioned, no set of parameters could be found that simultaneously gave large enough ρ_{00} and small enough differential cross sections. ($C_1=C_f=1$ gives ρ_{00} too small; $C_i \neq C_f \neq 1$ gives $d\sigma/d\Omega$ too large.) Thus the deficiencies of the OPEA model are inherent in the model and cannot be removed by a change in the values of the parameters.

The deficiencies of the absorption model may be due

TABLE VI. Decay angular correlations for K^*N^* production ($\cos\theta_{\text{c.m.}}>0.8$, 0.84 GeV$<M_{K^+\pi^-}<$0.94 GeV, 1.12 GeV$<M_{p\pi^+}<$1.32 GeV).

Parameter	Matrix elements	Angular functions	2.53 GeV/c (678 events)	2.76 GeV/c (1185 events)	3.20 GeV/c (1142 events)
$\rho_{00}^{K^*}$	$\Sigma_i R_{00;ii}$	$\frac{1}{2}\langle 5\cos^2\theta_{K^*}-1\rangle$	0.77±0.03	0.76±0.02	0.78±0.02
$\rho_{33}^{N^*}$	$\Sigma_i R_{ii;33}$	$\frac{1}{8}\langle 7-15\cos^2\theta_{N^*}\rangle$	0.07±0.02	0.06±0.02	0.10±0.02
$\rho_{1,-1}^{K^*}$	$\Sigma_i R_{1-1;ii}$	$-5/4\langle\sin^2\theta_{K^*}\cos 2\phi_{K^*}\rangle$	−0.04±0.02	−0.01±0.02	−0.04±0.02
$\mathrm{Re}\rho_{10}^{K^*}$	$\Sigma_i R_{10;ii}$	$-(5/4\sqrt{2})\langle\sin 2\theta_{K^*}\cos\phi_{K^*}\rangle$	−0.10±0.02	−0.13±0.01	−0.13±0.02
$\mathrm{Re}\rho_{3,-1}^{N^*}$	$\Sigma_i R_{ii;3-1}$	$-(5\sqrt{3}/8)\langle\sin^2\theta_{N^*}\cos 2\phi_{N^*}\rangle$	0.00±0.02	0.00±0.02	0.01±0.02
$\mathrm{Re}\rho_{31}^{N^*}$	$\Sigma_i R_{ii;31}$	$-(5\sqrt{3}/8)\langle\sin 2\theta_{N^*}\cos\phi_{N^*}\rangle$	−0.05±0.02	−0.03±0.02	−0.04±0.02
R_4	$R_{11;33}+R_{11;-3-3}-R_{11;11}$ $-R_{11;-1-1}-2R_{00;33}+2R_{00;11}$	$(25/8)\langle(1-3\cos^2\theta_{K^*})(1-3\cos^2\theta_{N^*})\rangle$	0.66±0.13	0.76±0.10	0.56±0.09
R_9	$R_{1-1;33}-R_{1-1;11}$	$-(25/16)\langle(1-3\cos^2\theta_{N^*})\sin^2\theta_{K^*}\cos 2\phi_{K^*}\rangle$	0.02±0.02	0.00±0.02	0.03±0.02
R_{10}	$R_{10;33}+R_{10;-3-3}-R_{10;11}-R_{10;-1-1}$	$-(25/8\sqrt{2})\langle(1-3\cos^2\theta_{N^*})\sin 2\theta_{K^*}\cos\phi_{K^*}\rangle$	0.08±0.05	−0.08±0.04	0.03±0.04
R_{11}	$R_{11;3-1}+R_{11;1-3}-2R_{00;3-1}$	$-(25\sqrt{3}/16)\langle(1-3\cos^2\theta_{K^*})\sin 2\theta_{N^*}\cos 2\phi_{N^*}\rangle$	−0.05±0.05	−0.01±0.04	−0.01±0.04
R_{12}	$R_{11;31}+R_{11;-1-3}-2R_{00;31}$	$-(25\sqrt{3}/16)\langle(1-3\cos^2\theta_{K^*})\sin 2\theta_{N^*}\cos\phi_{N^*}\rangle$	0.10±0.06	0.09±0.05	0.13±0.05
R_{13}	$R_{1-1;3-1}$	$(25\sqrt{3}/32)\langle\sin^2\theta_{K^*}\sin^2\theta_{N^*}\cos 2(\phi_{K^*}+\phi_{N^*})\rangle$	0.04±0.01	0.03±0.01	0.04±0.01
R_{14}	$R_{1-1;-13}$	$(25\sqrt{3}/32)\langle\sin^2\theta_{K^*}\sin^2\theta_{N^*}\cos 2(\phi_{K^*}-\phi_{N^*})\rangle$	0.02±0.01	−0.01±0.01	−0.01±0.01
R_{15}	$R_{1-1;31}$	$(25\sqrt{3}/32)\langle\sin^2\theta_{K^*}\sin 2\theta_{N^*}\cos(2\phi_{K^*}+\phi_{N^*})\rangle$	0.00±0.02	−0.01±0.01	0.00±0.01
R_{16}	$R_{1-1;13}$	$(25\sqrt{3}/32)\langle\sin^2\theta_{K^*}\sin 2\theta_{N^*}\cos(2\phi_{K^*}-\phi_{N^*})\rangle$	−0.02±0.02	0.01±0.01	0.02±0.01
R_{17}	$R_{10;3-1}+R_{10;1-3}$	$(25\sqrt{6}/32)\langle\sin 2\theta_{K^*}\sin^2\theta_{N^*}\cos(\phi_{K^*}+2\phi_{N^*})\rangle$	−0.00±0.03	−0.01±0.02	0.00±0.02
R_{18}	$R_{10;-31}+R_{10;-13}$	$(25\sqrt{6}/32)\langle\sin 2\theta_{K^*}\sin^2\theta_{N^*}\cos(\phi_{K^*}-2\phi_{N^*})\rangle$	−0.05±0.03	−0.01±0.02	0.01±0.02
R_{19}	$R_{10;31}-R_{10;-1-3}$	$(25\sqrt{6}/32)\langle\sin 2\theta_{K^*}\sin 2\theta_{N^*}\cos(\phi_{K^*}+\phi_{N^*})\rangle$	−0.05±0.03	0.01±0.02	−0.07±0.03
R_{20}	$R_{10;13}-R_{10;-3-1}$	$(25\sqrt{6}/32)\langle\sin 2\theta_{K^*}\sin 2\theta_{N^*}\cos(\phi_{K^*}-\phi_{N^*})\rangle$	0.01±0.03	0.02±0.02	−0.01±0.03

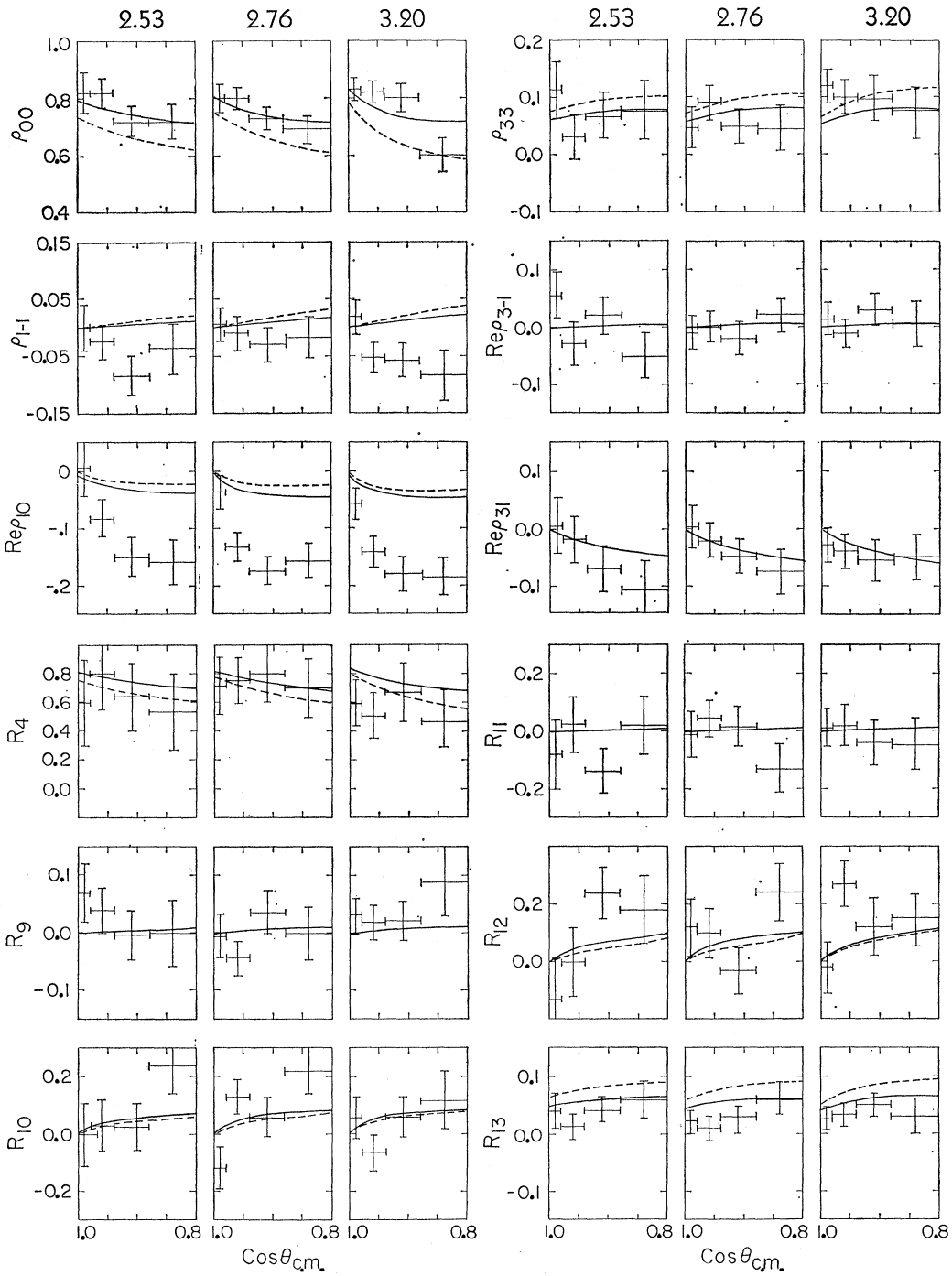

FIG. 10. Spin density-matrix elements ρ_{00}, $\rho_{1,-1}$, $\mathrm{Re}\rho_{10}$, ρ_{33}, $\mathrm{Re}\rho_{3,-1}$, $\mathrm{Re}\rho_{31}$, and K^*N^* joint decay coefficients R_4 and R_9-R_{13} as a function of K^* production cosine ($\cos\theta_{\mathrm{c.m.}}$) for the selected ($0.84<M_{K^+\pi^-}<0.94$ GeV, $1.12<M_{p\pi^+}<1.32$ GeV, and $\cos\theta_{\mathrm{c.m.}}>0.8$) double-resonance events. The solid (dashed) curves are the predictions of the OPEA model with parameters given by II (I) in Table V. Where only the solid curves are displayed, both parameter sets given identical predictions.

to two reasons. The absorption model assumes that the elastic scattering amplitude is completely imaginary and helicity nonchanging. At the energies considered in this experiment, the real part of the forward scattering amplitude could be as large as 40% of the imaginary amplitude.[37] In addition, the large value of polarization[45] observed near the forward direction in K^+p elastic scattering implies that the spin-flip amplitude

[45] N. E. Booth, G. Conforto, R. J. Esterling, J. Parry, J. Scheid, D. Sherden, and A. Yokosawa, Phys. Rev. Letters **23**, 192 (1969). J. G. Asbury, J. D. Dowell, S. Kato, D. Lundquist, T. B. Novey, A. Yokosawa, B. Barnett, P. F. M. Koehler, and P. Steinberg, Phys. Rev. Letters **23**, 104 (1969).

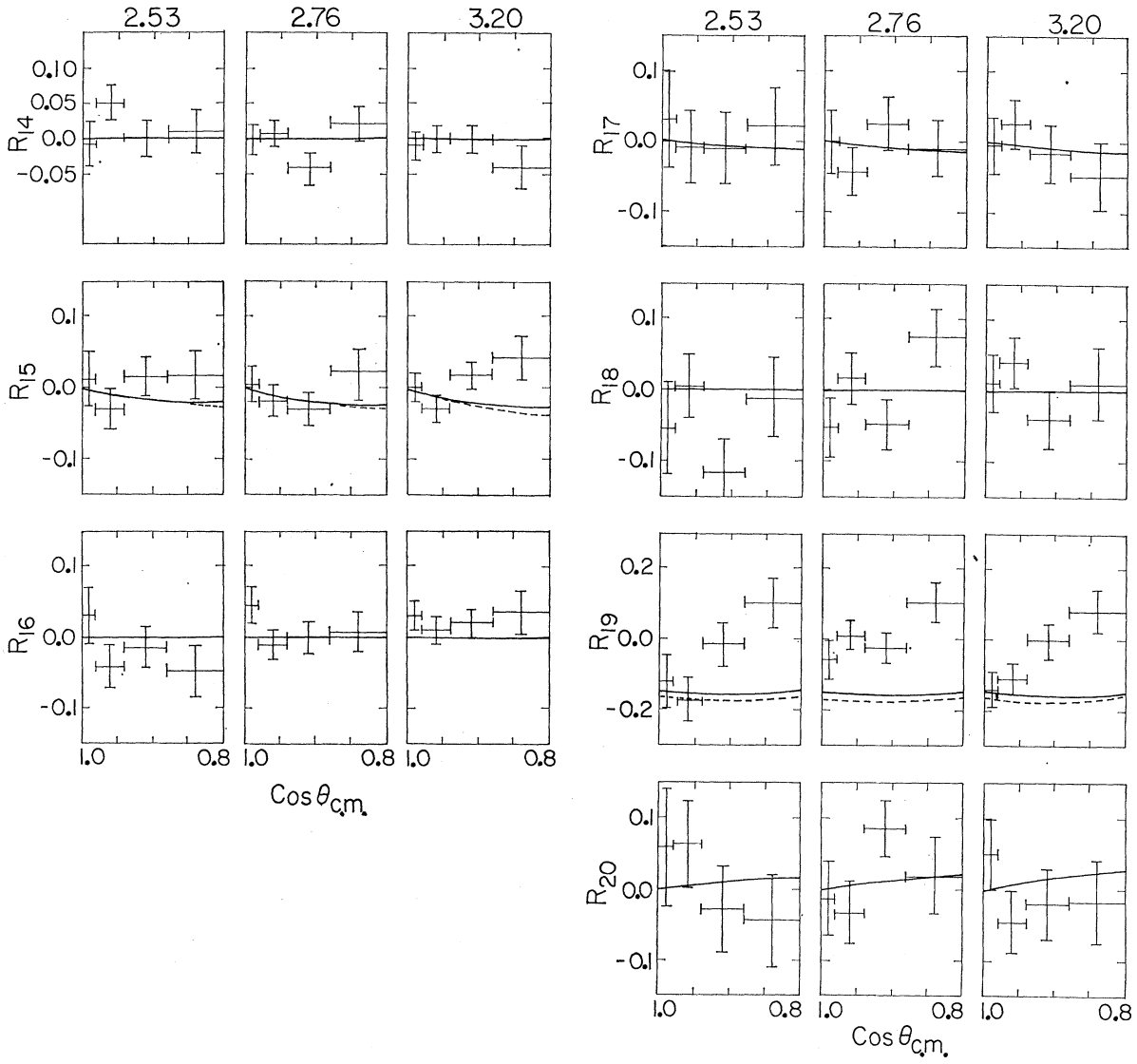

FIG. 11. K^*N^* joint decay coefficients $R_{14}-R_{20}$ as a function of K^* production cosine ($\cos\theta_{c.m.}$) for the selcted ($0.84<M_{K^+\pi^-}<0.94$ GeV, $1.12<M_{p\pi^+}<1.32$ GeV, and $\cos\theta_{c.m.}>0.8$) double-resonance events. The solid (dashed) curves are the predictions of the OPEA model with parameters given by II (I).

is not negligible. Jackson *et al.*[34] have also pointed out that the factorized form of the reaction amplitude is only valid when the range of the absorptive interactions satisfy $\sqrt{A_{i(f)}}\gg 1/m_x$, where $A_{i(f)}$ is the slope of the elastic scattering for particles in the initial (final) state and m_x is the mass of the exchange particle. This inequality is badly violated for π exchange.

C. Comparison with Quark-Model Predictions

The K^*N^* correlations also provide tests of the quark model. We have compared our data with the three classes of predictions derived by Białas and Zalewski.[46] These predictions have previously been studied in K^*N^*,[11] ρN^*, and ωN^* production at 5 GeV/c.[47] These predictions are most concisely expressed in terms of statistical tensors,[48] $T_{M_1M_2}{}^{J_1J_2}$, defined with the quantization direction (z axis) perpendicular to the production plane.[49] In terms of these tensors the three

[46] A. Białas and K. Zalewski, Phys. Letters **26B**, 170 (1968); Nucl. Phys. **B6**, 465 (1968).

[47] Bonn-Durham-Nijmegen-Paris-Strasbourg-Turin Collaboration, Phys. Letters **28B**, 72 (1968).

[48] A. Kotański and K. Zalewski, Nucl. Phys. **B4**, 559 (1968).

[49] The statistical tensors are defined in terms of spherical harmonics as follows: $T_{M0}{}^{20}=-(5\pi/6)^{1/2}<Y_2{}^M(\theta_{K^*},\phi_{K^*})>$, $T_{0N}{}^{02}=-(5\pi/3)^{1/2}<Y_2{}^N(\theta_{N^*},\phi_{N^*})>$, $T_{MN}{}^{22}=(\frac{2}{3})^{1/2}5\pi<Y_2{}^M(\theta_{K^*},\phi_{K^*})\,Y_2{}^N(\theta_{N^*},\phi_{N^*})>$.

classes of predictions are as follows:
Class I:

(a) $T_{00}^{20} - \sqrt{2}\, T_{00}^{02} = 0$,
(b) $\mathrm{Re}T_{20}^{22} - \frac{1}{2}\,\mathrm{Re}T_{20}^{20} = 0$,
(c) $\mathrm{Im}T_{20}^{22} - \frac{1}{2}\,\mathrm{Im}T_{20}^{20} = 0$,
(d) $\mathrm{Re}T_{02}^{22} - (1/\sqrt{2})\,\mathrm{Re}T_{02}^{02} = 0$,
(e) $\mathrm{Im}T_{02}^{22} - (1/\sqrt{2})\,\mathrm{Im}T_{02}^{02} = 0$,
(f) $T_{00}^{22} - 1/2\sqrt{6} + (1/\sqrt{2})T_{00}^{02} = 0$.

Class II:

(a) $\mathrm{Re}T_{20}^{20} - \sqrt{2}\,\mathrm{Re}T_{02}^{02} = 0$,
(b) $\mathrm{Im}T_{20}^{20} - \sqrt{2}\,\mathrm{Im}T_{02}^{02} = 0$,
(c) $\mathrm{Re}T_{20}^{22} - \mathrm{Re}T_{02}^{22} = 0$,
(d) $\mathrm{Im}T_{20}^{22} - \mathrm{Im}T_{02}^{22} = 0$,
(e) $\mathrm{Im}T_{2-2}^{22} = 0$,
(f) $\mathrm{Im}T_{1-1}^{22} = 0$.

Class III:

(a) $\mathrm{Im}T_{20}^{20} = 0$,
(b) $\mathrm{Im}T_{20}^{22} = 0$,
(c) $\mathrm{Im}T_{22}^{22} = 0$,
(d) $\mathrm{Im}T_{02}^{02} = 0$,
(e) $\mathrm{Im}T_{02}^{22} = 0$,
(f) $\mathrm{Im}T_{11}^{22} = 0$,
(g) $\mathrm{Re}T_{22}^{22} + \mathrm{Re}T_{2-2}^{22} + \mathrm{Re}T_{00}^{22} - 1/\sqrt{6} = 0$.

These classes differ in the number of assumptions made about the quark-quark scattering amplitude. The first class of predictions is derived by assuming that the initial- and final-state particles are composed of quarks in the usual way, and by assuming the standard property of additivity, which states that the particle-particle scattering amplitude is the coherent sum of the constituent quark-quark scattering amplitudes. (In the quark picture, the process $K^+p \to K^{*0}N^{*++}$ results from the charge-exchange process $\mathfrak{N}\mathcal{P} \to \mathcal{P}\mathfrak{N}$, where $\mathfrak{N}$ and $\mathcal{P}$ are the neutron- and protonlike quarks.) Only parity conservation is assumed to hold in quark-quark scattering. The predictions of classes II and III are obtained after making additional assumptions about the spin dependence of the quark-quark scattering amplitude. These predictions, which depend on invoking time-reversal invariance, are not as basic since they neglect the fact that the quarks are bound.

Predictions of class I are independent of the particular type of transverse frame chosen, while those of classes II and III cannot be satisfied in all transverse frames. In fact the class-III predictions can only hold in one transverse frame, while those of class II, if found to hold in one frame, will be satisfied in all frames differing only in a common rotation of K^* and N^*. Since the quark model does not specify in which frame the relations (of classes II and III) are to hold we have tested the relations in three transverse frames. We define the transverse Jackson frame by choosing the x axis as the direction of the beam (target) as seen in the K^* (N^*) rest frame, the transverse helicity frame by choosing the x axis as the direction of the line of flight of the K^* (N^*) in the over-all center-of-mass system as seen

TABLE VII. Statistical tensors for K^*N^* production ($\cos\theta_{\mathrm{c.m.}} > 0.8$, 0.84 GeV $< M_{K^+\pi^-} <$ 0.94 GeV, 1.12 GeV $< M_{p\pi^+} <$ 1.32 GeV; three energies combined 3005 events).

Statistical tensor	Transverse Jackson	Transverse helicity	Dynamic
T_{00}^{02}	0.098±0.011	0.098±0.011	0.098±0.011
T_{00}^{20}	0.152±0.007	0.152±0.007	0.152±0.007
T_{00}^{22}	0.105±0.016	0.105±0.016	0.105±0.016
$\mathrm{Re}T_{22}^{22}$	0.120±0.015	−0.076±0.015	0.126±0.015
$\mathrm{Im}T_{22}^{22}$	0.066±0.015	−0.066±0.015	−0.064±0.015
$\mathrm{Re}T_{2-2}^{22}$	0.089±0.015	0.089±0.015	0.089±0.015
$\mathrm{Im}T_{2-2}^{22}$	−0.009±0.015	−0.007±0.015	−0.007±0.015
$\mathrm{Re}T_{20}^{22}$	−0.057±0.014	−0.025±0.014	0.062±0.014
$\mathrm{Im}T_{20}^{22}$	−0.013±0.014	0.060±0.014	−0.014±0.014
$\mathrm{Re}T_{02}^{22}$	−0.084±0.012	−0.031±0.012	0.095±0.012
$\mathrm{Im}T_{02}^{22}$	−0.035±0.012	0.081±0.012	−0.015±0.012
$\mathrm{Re}T_{11}^{22}$	0.045±0.013	0.014±0.011	−0.040±0.013
$\mathrm{Im}T_{11}^{22}$	0.001±0.011	−0.034±0.013	0.017±0.011
$\mathrm{Re}T_{1-1}^{22}$	0.006±0.013	0.007±0.013	0.007±0.013
$\mathrm{Im}T_{1-1}^{22}$	−0.009±0.012	−0.009±0.012	−0.009±0.012
$\mathrm{Re}T_{02}^{02}$	−0.123±0.008	−0.031±0.009	0.123±0.008
$\mathrm{Im}T_{02}^{02}$	−0.033±0.009	0.113±0.009	−0.035±0.009
$\mathrm{Re}T_{20}^{20}$	−0.157±0.006	−0.097±0.006	0.184±0.006
$\mathrm{Im}T_{20}^{20}$	−0.088±0.006	0.142±0.006	0.00±0.007

TABLE VIII. Test of quark-model predictions for K^*N^* production ($\cos\theta_{\mathrm{c.m.}} > 0.8$, 0.84 GeV $< M_{K^+\pi^-} <$ 0.94 GeV, 1.12 GeV $< M_{p\pi^+} <$ 1.32 GeV; three energies combined, 3005 events).

Relation	Transverse Jackson	Transverse helicity	Dynamic
I-a	0.014±0.017	0.014±0.017	0.014±0.017
I-b	0.021±0.013	0.024±0.013	−0.030±0.013
I-c	0.031±0.013	−0.011±0.013	−0.014±0.014
I-d	0.003±0.011	−0.008±0.011	0.008±0.011
I-e	−0.011±0.011	0.001±0.012	0.010±0.011
I-f	−0.030±0.020	−0.030±0.020	−0.030±0.020
II-a	0.018±0.013	−0.053±0.014	0.010±0.013
II-b	−0.041±0.014	−0.017±0.013	0.049±0.014
II-c	0.026±0.018	0.006±0.018	−0.033±0.018
II-d	0.022±0.018	−0.021±0.018	0.002±0.019
II-e	−0.009±0.015	−0.007±0.015	−0.007±0.015
II-f	−0.009±0.012	−0.009±0.012	−0.009±0.012
III-a	−0.088±0.006	0.142±0.006	−0.0±0.007
III-b	−0.013±0.014	0.060±0.014	−0.014±0.014
III-c	0.066±0.015	−0.066±0.015	−0.064±0.015
III-d	−0.033±0.009	0.113±0.009	−0.035±0.009
III-e	−0.035±0.012	0.081±0.012	−0.015±0.012
III-f	0.001±0.011	−0.034±0.013	0.017±0.011
III-g	−0.095±0.027	−0.290±0.027	−0.089±0.027

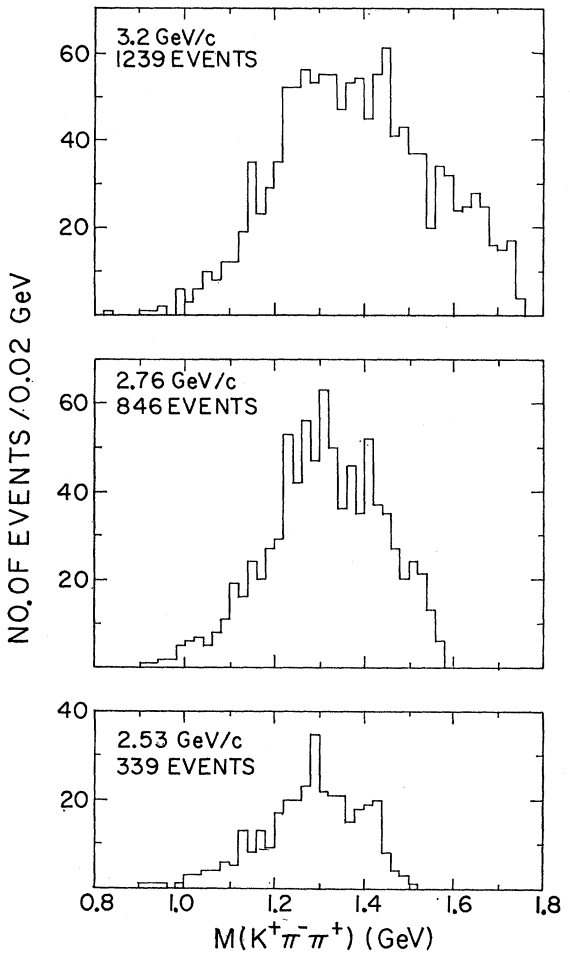

FIG. 12. Distribution of mass of $K^+\pi^+\pi^-$ system at each energy for those events with N^{*++} removed ($M_{p\pi+}>1.4$ GeV).

in the K^* (N^*) rest frame, and the "dynamic" frame by a common rotation from the transverse Jackson frame so that the condition $\mathrm{Im}T_{20}^{20}=0$ is satisfied (Donohue-Högaasen frame).[50] A detailed study at 5 GeV/c showed that for K^*N^* production reference systems could be found in which the quark relations are satisfied, in agreement with ρN^* data, but in disagreement with ωN^* data.

The statistical tensors were evaluated in each of the frames at the three momenta by the method of moments and found to be independent of momentum for $\cos\theta_{\mathrm{c.m.}}>0.8$ (as expected from the study of K^*N^* correlations). Our results are summarized in Tables VII and VIII. We find reasonable agreement for class-I and -II relations in all three coordinate systems. We note that for the events considered the rotations from transverse Jackson to transverse helicity are almost identical for K^* and N^*. Slightly better agreement is obtained for the narrower mass cuts $0.89<K^*<0.91$ GeV and $1.17<\mathrm{N}^*<1.27$ GeV (not shown). However, we find (independent of mass cuts used) that relations of class III are not satisfied in any of the three coordinate systems tried. As seen in Table VIII, the best results for class-III relations are obtained in the Donohue-Högaasen frame. Three relations, however, are more than 3 standard deviations from being satisfied. For comparison, we note that although the CERN group calls the agreement at 5 GeV/c with class-III predictions reasonable, the same discrepancies (with less statistical significance) appear in their data.

V. ANALYSIS OF THE Q REGION

Previous experiments have established the existence of a low-mass $K\pi\pi$ enhancement near 1.3 GeV.[16–23,51–54]

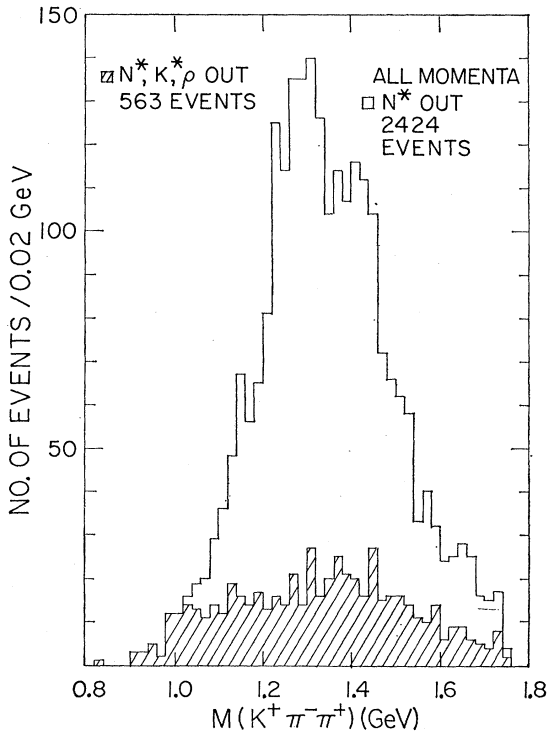

FIG. 13. Distribution of mass of $K^+\pi^+\pi^-$ system, all three energies combined, for those events with N^{*++} removed ($M_{p\pi+}>$ 1.4 GeV). The cross-hatched histogram corresponds to those events in which N^*, K^*, and ρ have been removed ($M_{p\pi+}>$ 1.4 GeV, $M_{K+\pi-}>0.94$ GeV or <0.84 GeV, $M_{\pi+\pi-}>0.80$ GeV or <0.62 GeV).

[50] J. T. Donohue and H. Högaasen, Phys. Letters **25B**, 554 (1967). At each energy the data were divided into the four $\cos\theta_{\mathrm{c.m.}}$ intervals that were used to display the correlation coefficients. For each interval an average rotation angle from the transverse Jackson to the dynamic frame was obtained. Each event was then rotated by the angle appropriate to its value of $\cos\theta_{\mathrm{c.m.}}$.

[51] J. Andrews, J. Lach, T. Ludlam, J. Sandweiss, H. D. Taft, and E. L. Berger, Phys. Rev. Letters **22**, 731 (1969).

[52] J. C. Park, S. Kim, G. Chandler, G. Ascoli, E. L. Goldwasser, and T. P. Wangler, Phys. Rev. Letters **20**, 171 (1968).

[53] P. J. Dornan, V. E. Barnes, G. R. Kalbfleisch, I. O. Skillicorn, M. Goldberg, B. Goz, R. Wolfe, and J. Leitner, Phys. Rev. Letters **19**, 271 (1967).

[54] D. J. Crennell, G. R. Kalbfleisch, K. W. Lai, J. M. Scarr, and T. G. Schumann, Phys. Rev. Letters **19**, 44 (1967).

A study of this mass region is complicated at the low energies of this experiment by the strong $N^*(1236)$ production which accounts for $\sim\frac{2}{3}$ of the cross section of this final state. In order to remove the effects of the $N^*(1236)$, we only consider in this section events with $M(p\pi^+)>1.4$ GeV (N^* out). In Fig. 12 we show the $K^+\pi^+\pi^-$ mass distribution at each energy with the N^* events removed. No significant substructure in the Q region is apparent for any momentum. In an effort to reduce statistical fluctuations, we have consolidated the three momenta in Fig. 13. A shoulder near 1.4 GeV is present [presumably associated with the $K^*(1420)$]. A noteworthy feature of the data is the relatively clean appearance of a peak centered at 1.3 GeV. As may be seen from the shaded histrogram in Fig. 13, the Q enhancement disappears completely when events outside the $K^*(890)$ and ρ^0 bands (840–940 and 620–800 MeV) are plotted. It should be emphasized that it is necessary to remove the ρ^0 events in order to obtain the smooth background in Fig. 13.

A significant contribution to the enhancement at 1.3 GeV may arise from the Deck mechanism.[55] The K^{*0} events produced by the mechanism are expected to show the normal $\cos^2\theta_{K^*}$ distribution and a flat Treiman-Yang angular distribution. In Fig. 14 we compare the distribution of $\cos\theta_{K^*}$ obtained when the momentum transfer Δ^2 between the initial- and final-state protons is less than and greater than 0.3 $(\mathrm{GeV}/c)^2$. While the Treiman-Yang distribution (not shown) is uniform for both selections, the $\cos\theta_{K^*}$ distribution is almost pure $\cos^2\theta$ (with an asymmetry similar to that noted in K^*N^* production) for small values of Δ^2. In contrast, the $\cos\theta_{K^*}$ distribution at large Δ^2 has a large isotropic component and displays no asymmetry. For comparison, we have made the same Δ^2 cuts for K^*N^* and $K\pi N^*$ and find the asymmetry to be present in both cases.

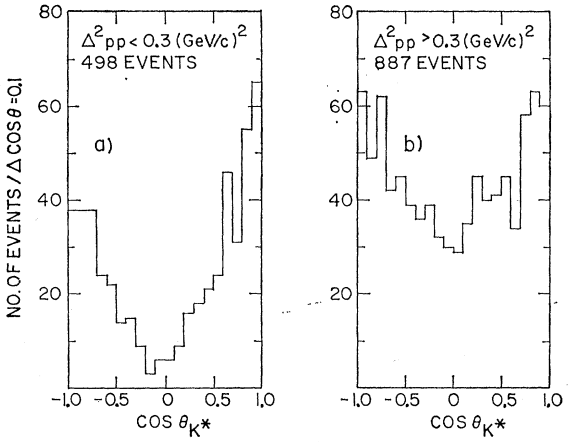

FIG. 14. (a) Distribution of K^* ploar decay cosine ($\cos\theta_{K^*}$), all three energies combined, for those events with K^* in ($0.84<M_{K^+\pi^-}<0.94$ GeV), N^* out ($M_{p\pi^+}>1.4$ GeV), and $\Delta_{p,p}{}^2<0.3$ $(\mathrm{GeV}/c)^2$. (b) Distribution of K^* polar decay cosine ($\cos\theta_{K^*}$), all three energies combined, for those events with K^* in (0.84 GeV$<M_{K^+\pi^-}<0.94$ GeV), N^* out ($M_{p\pi^+}>1.4$ GeV), and $\Delta_{p,p}{}^2>0.3$ $(\mathrm{GeV}/c)^2$.

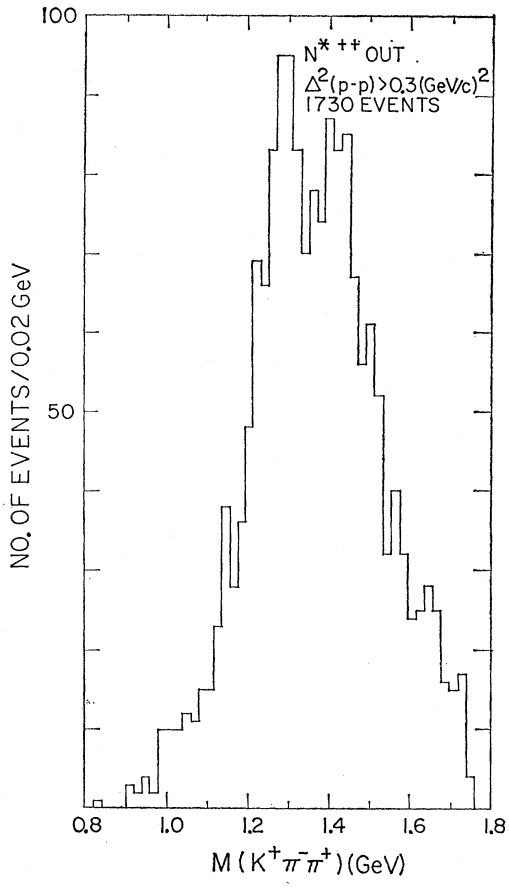

FIG. 15. Distribution of mass of $K\pi\pi$ system, all three energies combined, for those events with N^{*++} out ($M_{p\pi+}>1.4$ GeV) and $\Delta_{p,p}{}^2>0.3$ $(\mathrm{GeV}/c)^2$.

We therefore impose a $\Delta^2>0.3$ $(\mathrm{GeV}/c)^2$ cut on the data and present the result in Fig. 15. The peak at 1300 MeV [henceforth called the $K^*(1300)$] is a 4-standard-deviation enhancement above background and is well separated from the $K^*(1420)$. The $K^*(1420)$ signal is centered at 1430 ± 10 MeV with a width of 80 ± 20 MeV in good agreement with compiled values. The $K^*(1300)$ is estimated to have a mass of 1300 ± 10 MeV and a width of 80 ± 20 MeV. The mass and width of the $K^*(1300)$ are consistent with those observed in K^+p at 4.6 GeV/c [20] and in π^-p at 6.0 GeV/c.[53]

We have attempted to determine the dominant spin-parity states in the region of the $K^*(1300)$. For this analysis we have neglected the effects of background and any other possible decay modes of the $K^*(1300)$ other than $K^*\pi$. The method is that of Park and Kim,[56] in which the ratios of moments of polar angles associated with the normal to the three-body decay plane and the K^* helicity axis, which are independent of pro-

[55] R. T. Deck, Phys. Rev. Letters **13**, 169 (1964).

[56] J. C. Park and S. Kim, Phys. Rev. **174**, 2165 (1968).

duction mechanism, are used to determine the spin and parity. Park and Kim have shown that the ratio

$$R=\langle P_2(\cos\theta_1)\rangle/\langle P_2(\cos\beta)\rangle$$

is given by

$$1-3f_0 \quad \text{for } 1^+$$

$$(1+f_0)/(f_0-2) \quad \text{for } 2^-$$

and

$$(6+2f_0)/(5f_0-9) \quad \text{for } 3^+.$$

θ_1 is the polar angle of the K^* line of flight and β is the polar angle of the normal to the three-body decay plane as measured in the $K^*(1300)$ rest system with the z axis defined by the incident K^+; f_0 is the (0, 0) component of the K^* density matrix in the helicity representation. The nonzero value observed for f_0 excludes the natural spin-parity series 1^-, 2^+, ... ($f_0=0.43\pm 0.06$ for the mass region 1.2–1.4 GeV). We have performed this analysis on the combined data and find that the data in the region 1.2–1.4 GeV are less than 1 standard deviation from being consistent with 1^+ while the data are 1.7 and 2.1 standard deviations from being consistent with 2^- and 3^+, respectively.[57]

In examining the $K\pi\pi$ mass distributions, we have found it necessary to remove events in the ρ^0 mass region ($620<M_{\pi\pi}<800$ MeV) in order to obtain a smooth background in the $K^*(1300)$ region. It should be noted that in order to obtain a statistically significant signal for the $K^*(1300)$ we have had to combine the three incident beam momenta. The combination of the three momenta, in addition to the cuts that were necessary to remove the Deck effect and the $N^*(1236)$, makes a study of the $K^+\rho^0$ decay mode extremely difficult.

VI. SEARCH FOR THE Z*

The momenta used for this exposure were selected to examine the enhancement at 2505 MeV in the K^+p total cross section reported by Abrams *et al.*[1] The enhancement could be due either to threshold effects or to the production of a resonance, the $Z^*(2505)$. The resonance interpretation implies a production cross section of 0.2 mb and a value of $(J+\frac{1}{2})\kappa$ of 0.04, where J and κ are the spin and elasticity of the resonance.

We have searched for evidence of the existence of this resonance by examining the quasi-two-body final states in the four-body and other topologies at these energies. Except for a possible anomaly in backward elastic scattering,[58] we have found no evidence for resonantlike behavior. For example, the spin density-matrix elements for the $K^*(890)$ $N^*(1236)$ final state agree with those reported at higher energies. We also do not observe any significant behavior in the backward hemisphere which might be expected for the quasi-two-body decay of a resonance of definite spin and parity.

If the enhancement is due to threshold behavior we are unable to find any single channel whose energy dependence reflects the observed behavior of the total cross section. It is clear that there are many candidates [e.g., the $K^*(1300)$, the $K^*(1420)$, and several nucleon isobars], but none of them exhibit any strong energy dependence in this energy region.

ACKNOWLEDGMENTS

We would like to acknowledge the help of Dr. L. Voyvodic, Dr. F. Schweingruber, and the Argonne National Laboratory 30-in. bubble-chamber crew during the experimental exposure. We would also like to thank Professor E. L. Goldwasser for his participation during the initial states of this experiment. At various stages during this analysis we have benefited from discussions with Professor B. I. Eisenstein, Professor L. M. Jones, and Professor J. S. Trefil. Finally, we would like to thank the scanners and measurers at the University of Illinois for their conscientious efforts during all phases of this experiment.

[57] If the analysis is performed on the combined data without the Δ^2 cut we are 2 standard deviations from 1^+ and more than 6 standard deviations from 2^+ and 3^-. We have noted, however, that the K^* angular distributions indicate that the low Δ^2 distributions have significant one-pion-exchange production of the $K^*(890)$.

[58] G. S. Abrams, L. Eisenstein, T. A. O'Halloran, Jr., W. Shufeldt, and J. Whitmore, Phys. Rev. Letters **21**, 1407 (1968); G. S. Abrams, L. Eisenstein, J. Kim, T. A. O'Halloran, Jr., W. Shufeldt, and J. Whitmore, University of Illinois Report No. COO-1195-156, 1969 (unpublished).